Experimental characterisation and verification of a base-isolation system including fluid viscous spring-dampers

EUROPEAN COMMISSION
DIRECTORATE-GENERAL
Joint Research Centre

Institute for the Protection and Security of the Citizen

University of Udine

Experimental Characterisation and Verification of a Base-Isolation System Including Fluid Viscous Spring-Dampers

S. Sorace
University of Udine

G. Terenzi
University of Florence

F. J. Molina, G. Magonette
Joint Research Centre, European Laboratory for Structural Assessment

Institute for the Protection and Security of the Citizen

2006

EUR 22147 EN

European Commission
Directorate-General Joint Research Centre
Institute for the Protection and Security of the Citizen

Contact information
Address: via Enrico Fermi, 1, 21021 Ispra (VA), Italy
E-mail: francisco.molina@jrc.it
Tel.: +39 0332786069
Fax: +39 0332789049

http://elsa.jrc.it/
http://www.jrc.cec.eu.int

EUR 22147 EN
Luxembourg: Office for Official Publications of the European Communities

Printed in Italy

ABSTRACT

An experimental investigation was carried out on an advanced seismic protection system incorporating base isolators and supplemental damping devices. This testing campaign was part of the Research Programme DISPASS (Dissipation and ISolation PAssive Systems Study), financed under the ECOLEADER contract within the Fifth Framework Program of the European Commission. The protection strategy considered herein consists in coupling stainless steel-Teflon bearings, operating as sliders, and silicone fluid viscous spring-dampers. The latter are connected to the base-floor of the isolated building to provide the desired passive control of superstructure response, as well as to guarantee its complete re-centring after termination of a seismic action. Two types of experiments were conducted: sinusoidal and random cyclic tests, and a pseudodynamic test in "substructured" configuration. The cyclic tests were aimed at characterising the hysteretic response of the spring-dampers, the frictional behaviour of the steel-Teflon bearings, and the combined response of their assembly. The pseudodynamic test simulated the installation of the protection system at the base of a three-story steel frame structure, physically tested in other tasks of the DISPASS Project in unprotected conditions, as well as by equipping it with different passive control technologies. The results of the performed tests, as well as of relevant mechanical interpretation and numerical simulation analyses, are presented in this report.

1 INTRODUCTION

The DISPASS Project was developed at the ELSA laboratory and involved the University of Udine as the co-ordinating unit, and the Universities of Florence and Kassel as participants. The Project was dedicated to the experimental investigation of three advanced seismic protection technologies for building structures, namely: a damped bracing system incorporating silicone fluid viscous (SFV) devices (Udine and Florence); the HYDE (HYsteretic DEvice) system (Kassel); and a combined base isolation/supplemental damping (BISD) system, coupling stainless steel-Teflon bearings and SFV spring-dampers (Udine and Florence).

The latter technology has been studied for many years by the research groups of Florence and Udine Universities (Terenzi, 1999; Chiarugi et al., 2000, 2001; Sorace and Terenzi, 2001a, b). The experimental characterisation of SFV devices, the analytical and numerical modelling of their response as well as of steel-Teflon sliders', and the definition of design criteria for an optimal implementation of the system, were particularly developed within these studies. A first experimental verification of the system performance was also carried out at the Structural laboratory of the University of Florence, by installing it on a 1:4-scale steel mock-up subjected to a dynamic vibration testing campaign (Chiarugi et al. 2000, Sorace and Terenzi, 2001a). These tests were aimed at checking the prediction capabilities of the analytical equation supporting the design procedure formulated in (Sorace and Terenzi, 2001a). Response data satisfactorily validated this equation.

With a view to proceed to a first installation of the BISD system on an actual structure, i.e. a reinforced concrete public building in Florence (Sorace and Terenzi, 2004, 2005), a more extensive experimental enquiry was planned within the DISPASS Project. The objectives of this testing programme, developed by a new experimental apparatus expressly set up at the ELSA laboratory, were: a methodical evaluation of the effects of

normal load and strain rate on the frictional behaviour of the last generation of steel-Teflon sliding bearings, manufactured in compliance with the requirements of the most recent edition of the Italian National Standards (CNR 10018, 1999) and European pre-Standards (prEN 1337, 2003) for this class of devices; a further enquiry of strain rate effects on the response of SFV spring-dampers for their best compensation in pseudodynamic tests, by examining devices whose dimensions are typical of base isolation applications, rather than of damped bracing designs (as the elements tested in the first task of DISPASS – Molina et al., 2004); a laboratory installation of a complete BISD system, to be subjected (a) to cyclic characterisation tests, in order to examine the interference of the frictional response of steel-Teflon sliders with the damping action of SFV dissipaters, and (b) to a substructured pseudodynamic verification test, to survey the system performance under a realistic and severe earthquake simulation.

The reference structure for the pseudodynamic test was a 2:3 scale three-story double steel frame, already tested in previous stages of the DISPASS Project, both in unprotected conditions and by equipping it with different protection techniques (SFV-damped braces – Sorace and Terenzi, 2003, Molina et al. 2004; and the HYDE system – Schmidt et al., 2004). This structure, shown in Figure 1, has 4 m-long spans and 2 m-high stories. Columns and beams are in HEB 140 and IPE 180 profiles, respectively. Beam-to-column connections are welded and stiffened by horizontal plates, which extend the beam flanges within the joint panels. The floors are made of steel-concrete composite slabs, clamped to beams by headed shear connectors.

Figure 1. Reference steel structure

The design of the BISD system for its application to the mock-up structure; the characteristics of the experimental apparatus for the cyclic tests on the BISD components and their assemblies, as well as for the pseudodynamic test on the complete system; a description of the substructured pseudodynamic testing method; and the results of the various stages of the experimental programme, relevant elaborations, interpretation and numerical simulations, are particularly presented in the next sections.

2 DESIGN OF SFV SPRING-DAMPERS AND STEEL-TEFLON SLIDERS

The design of the spring-dampers was carried out in the hypothesis of placing a pair of single-acting opposite devices at the base of each frame constituting the reference steel structure. One of the two twin frames, with relevant splitted masses, was then tested in the substructured pseudodynamic experiment. Moreover, the device pistons were positioned at their half-stroke, so as to obtain a symmetrical double-acting combined response of the pair of single-acting elements.

The damping coefficient c of each of the two single-acting spring-dampers was determined by the design equation formulated in (Sorace and Terenzi, 2001a) for a single-degree-of-freedom dynamic model of the base-isolated building, whose superstructure is idealised as a rigid mass. This equation has the following form:

$$c(\eta, \varphi, A_i) = c_{0.1}(\eta, A_i)\frac{(1+\vartheta)^{\gamma}}{[(1-\varphi^2)^2+\eta^2]^{\gamma}} \tag{1}$$

where c is the damping coefficient; η is the loss factor, expressed as:

$$\eta = \frac{E_d}{2\pi E_e} \tag{2}$$

being E_d the dissipated energy and E_e the stored energy; φ is the frequency ratio (i.e., the ratio of the harmonic load frequency – or the lower frequency in the main spectral composition of the input accelerogram, f_{lp}, in the case of seismic analyses – to the oscillator frequency); A_i is the peak input acceleration; $c_{0.1}$ is the damping coefficient calculated as the value to obtain η under the action of a sinusoidal input with amplitude A_i, and frequency 1/10 of the fundamental vibration frequency of the base-isolated system, f_{is}; and θ, γ are tuning coefficients, calibrated in (Sorace and Terenzi, 2001a) for a wide range of η factors. Once the target η value is fixed, expression (1) provides a quick evaluation of the extreme c value that can theoretically be demanded to the damper by imposing the resonant condition $\varphi = 1$, or a near-resonant condition, whatever the type of deterministic or random dynamic action with peak amplitude A_i.

Application of equation (1) starts from fixing the fundamental vibration frequency f_{is} in base-isolated conditions. Within this design, f_{is} was targeted by assuming a rounded value 3 for the f_{fb}/f_{is} ratio, where f_{fb} is the fundamental vibration frequency in fixed-base conditions of the steel structure, equal to 2.27 Hz (corresponding to a fundamental vibration period T_{fb} = 0.44 s). Then, f_{is} = 0.704 Hz (vibration period T_{is} = 1.42 s) was assumed. Further choices of the parameters included in (1) were: η = 0.5 (corresponding to an equivalent viscous damping ratio ξ = 0.25); φ = 1.14, as obtained by assuming a f_{lp} value of 0.8 Hz, as suggested for Eurocode 8-generated artificial accelerograms. Then, the computed $c_{0.1}(\eta, A_i)$ coefficient was equal to 3.96 kN(s/mm)$^{\alpha}$, where α is the fractional exponent – ranging from 0.1 to 0.2 (in this case equal to 0.15) – of the analytical relation expressing the damping restoring force F_d of a SFV spring-damper:

$$F_d(t) = c \cdot |v(t)|^{\alpha} \cdot \mathrm{sign}(x(t)) \tag{3}$$

being $v(t)$ the piston velocity, function of the time variable t.

Based on the established values of the parameters included in (1), the following preliminary design damping coefficient was obtained for the pair of devices:

$c(\eta, \varphi, A_i) = 6.1 \text{ kN}(\text{s/mm})^{\alpha}$.

This represents the median of the values calculated for five artificial accelerograms assumed in the design analysis, generated from the response spectrum of Eurocode 8, one of which was also used as input in the pseudodynamic test (Figure 2).

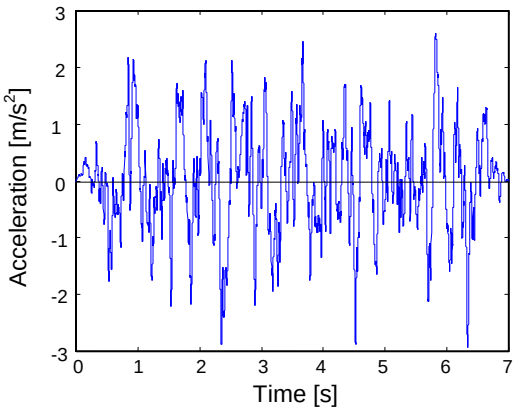

Figure 2. Input accelerogram for the pseudodynamic test

The "spring" characteristics of each SFV element were defined as follows:

$k_2 = 4\pi^2 \cdot f_{is}^2 \cdot M_i = 0.178 \text{ kN/mm}$,

where M_i is the building mass relevant to each device, equal to 9.11 kg;

$k_1 = 15k_2 = 2.67 \text{ kN/mm}$.

The static pre-load F_0 applied in the manufacturing phase was fixed by the empirical formula (Sorace and Terenzi, 2001a)

$$F_0 = \frac{k_2 \cdot d_{max}}{5} = 7.1 \text{ kN}$$

where d_{max} is the maximum device stroke, set as equal to 200 mm to obtain a ±100 mm operational displacement after the initial half-stroke positioning of the piston. These k_1, k_2 and F_0 values completely defined also the non-linear elastic restoring force F_e of the spring-dampers

$$F_e(t) = k_2 \cdot x(t) + \frac{(k_1 - k_2) \cdot x(t)}{\left[1 + \left|\frac{k_1 x(t)}{F_0}\right|^5\right]^{1/5}} \qquad (4)$$

where x is the piston displacement.

As final design choice, two XLR 12-200 spring-dampers were selected from the Jarret catalogue, providing the best approximation of the preliminary design k_1, k_2 and F_0 values determined above. The nominal energy dissipation capacity E_n of these devices is equal to 12 kJ, which also determines the maximum attainable c coefficient. The specific c value requested in the design phase can be imposed, within the capacity limit expressed by E_n, by properly calibrating the piston bore of the device.

It is worth noting that, being any pair of SFV devices connected in parallel within a BISD system, the resulting k_2, k_1 and c parameters for the coupled elements are twice the values of each device. Thus, the global design values for the two spring-dampers are: $k_{2t} = 0.356$ kN/mm; $k_{1t} = 5.34$ kN/mm; $c_t = 12.2$ kN(s/mm)$^{\alpha}$.

The design of the steel-Teflon sliding bearings was carried out by assuming to limit the maximum normal pressure within 10 N/mm^2. By considering a maximum vertical load of 137.5 kN for each device, the area of the circular Teflon disks (shown in Figure 3 during the lubrication phase) was fixed at 15000 mm^2. The corresponding diameter is 138 mm. The austenitic steel plates have dimensions of 500x250 mmxmm, with a thickness of 4 mm. The remaining technical details were consistent with the prescriptions of CNR-10018 (1999) and prEN-1337 (2003).

Figure 3. Two Teflon disks during the lubrication phase

3 CYCLIC TESTS – RESULTS AND ELABORATIONS

The following series of cyclic tests were performed:

1. on a single XLR 12-200 spring-damper;
2. on the two XLR 12-200 spring-dampers in pair;
3. on the steel-Teflon sliding bearings;
4. on the assembled system of spring-dampers and sliding-bearings.

The experimental results and relevant elaborations are presented in the following subsections for each type of test.

3.1 Tests on a single SFV spring-damper

The tests were carried out by imposing the displacement time-history plotted in Figure 4 on each XLR 12-200 device. Six tests were performed (named LR1 → LR6) by scaling the time axis by a factor λ ranging from 1 (as shown in Figure 4) to 3, 5, 30, 100, and 300. The corresponding maximum velocities v_{max} varied from 126 mm/s (λ = 1) to 0.42 mm/s (λ = 300).

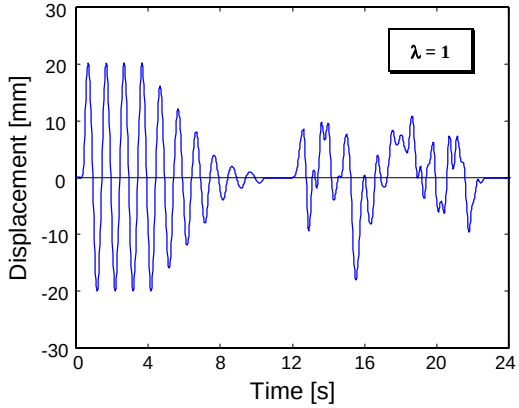

Figure 4. Input displacement time-history for the cyclic tests

As way of example of the experimental results, the response cycles obtained from tests with λ equal to 1, 30, and 300 are plotted in Figure 5. A progressive reduction of the total reaction force F (given by the sum of F_d and F_e) – and thus of the energy dissipation capacity – emerges from these graphs, as a consequence of the strain rate effects featuring this class of devices.

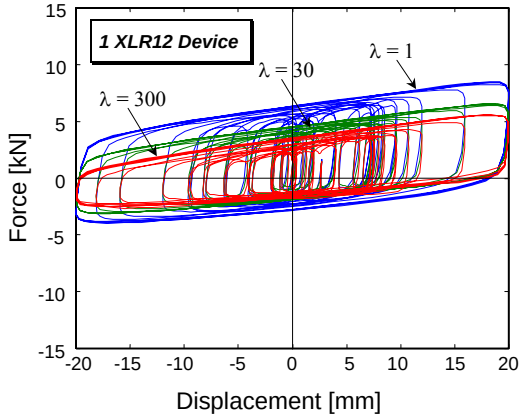

Figure 5. Response cycles obtained from tests with λ = 1, 30, 300

The experimental data were elaborated to evaluate the dissipated energy E_d, the ΔE_d energy dissipation decrease in passing from test with λ = 1 to the remaining tests ($\Delta E_d = [E_{d,\lambda=1} - E_{d,\lambda=\lambda i}]/E_{d,\lambda=1}$, where λ_i denotes a generic λ value different from 1), and the damping coefficient c_1 (where index 1 refers to the response of a single device). The results of these computations are summed up in Table 1, along with the imposed maximum velocity v_{max}, and the maximum reaction force values F_{max} measured in the tests.

Table 1. Test results and computed data

Test	λ	v_{max} (mm/s)	F_{max} (kN)	E_d (kN·mm)	ΔE_d (%)	c_1 (kN(s/mm)$^{\alpha}$)
LR1	1	126	9.01	$3.30 \cdot 10^3$	–	2.37
LR2	3	42	8.50	$2.96 \cdot 10^3$	10.3	2.53
LR3	5	25.2	8.24	$2.79 \cdot 10^3$	15.4	2.57
LR4	30	4.2	6.54	$2.22 \cdot 10^3$	32.7	2.72
LR5	100	1.26	5.97	$1.94 \cdot 10^3$	41.2	2.84
LR6	300	0.42	5.56	$1.73 \cdot 10^3$	47.6	2.94

The ΔE_d data in Table 1 underline the rate-sensitivity of SFV devices, with damping energy reductions ranging from around 10%, for $\lambda = 3$, to around 50%, for $\lambda = 300$. This confirms the results of previous enquiries on these effects (Molina et al., 2004), and thus the need for a proper compensation in seismic experiments performed over an expanded time-scale, such as pseudodynamic tests. The damping coefficient values are moderately influenced by the strain-rate effects since, according to (3), E_d decreases as velocity does.

The tests were reproduced numerically by the model defined by relations (3) and (4). The satisfactory correlation between experimental and numerical responses is illustrated in Figure 6, where the total restoring force time-histories, and the corresponding force-displacement cycles are demonstratively plotted, in superposition, for test with $\lambda = 5$.

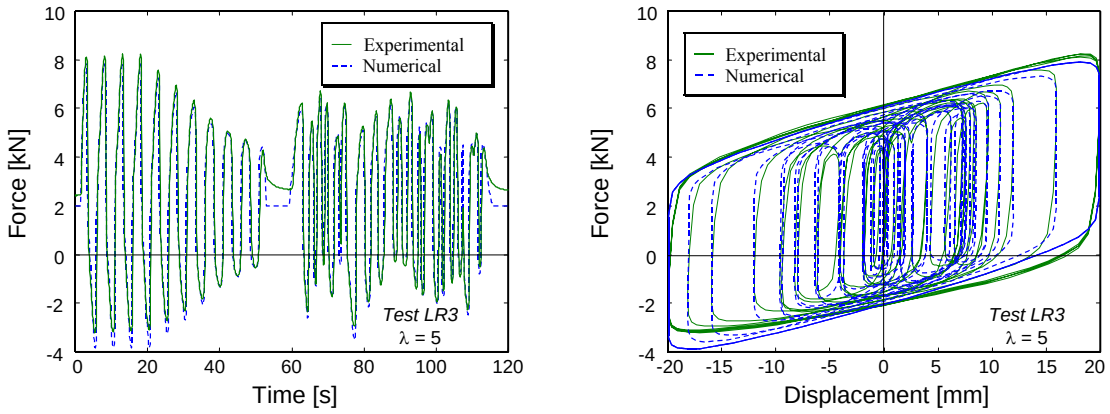

Figure 6. Experimental and numerical reaction force time-histories and force-displacement cycles, for LR3 test

3.2 Tests on a pair of SFV spring-dampers

3.2.1 First series of tests

The front view and the plan of the experimental apparatus implemented to carry out the cyclic and pseudodynamic tests on the BISD system and its components, are illustrated in Figure 7. A photographic view of the apparatus, and a detailed view of the two XLR 12-200 devices in "pull-push" configuration (i.e., with both pistons positioned at half-stroke), are shown in Figures 8 and 9, respectively.

During the tests on the two SFV devices, no vertical loads were applied on the upper beam of the apparatus, so as to avoid spurious damping contributions of the steel-Teflon sliding bearings. The displacement time-history in Figure 4 was imposed also in these tests, but with amplitudes divided by 2. Therefore, the maximum velocities resulted to be one-half the values reached in the corresponding tests performed on the single XLR 12-200 device.

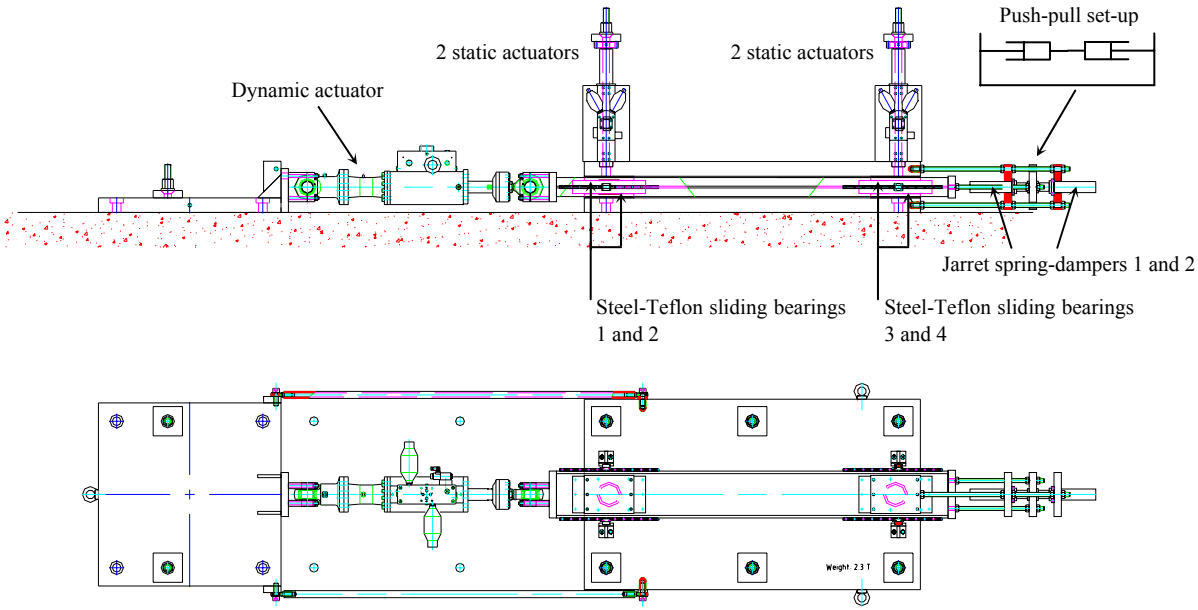

Figure 7. Front view and plan of the experimental apparatus

Figure 8. Photographic view of the experimental apparatus

Figure 9. Detailed view of the XLR 12-200 spring-dampers in push-pull configuration

Similarly to the graphs in Figure 5, Figure 10 shows the response cycles obtained from tests with λ = 1, 30, and 300. The results of the six tests are recapitulated in Table 2 by the same parameters used in Table 1.

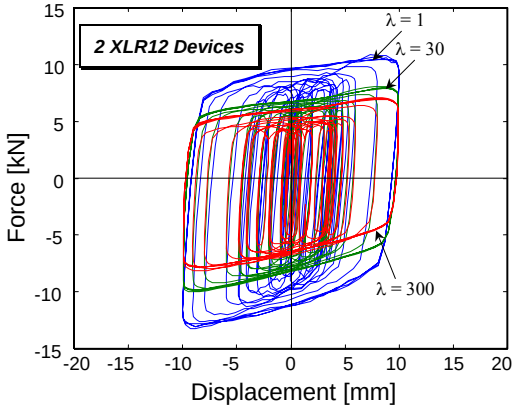

Figure 10. Response cycles obtained from tests with λ = 1, 30, 300

Table 2. Test results and computed data

Test	**λ**	v_{max} (mm/s)	F_{max} (kN)	E_d (kN·mm)	ΔE_d (%)	c_2 (kN(s/mm)$^{\alpha}$)
LR1a	1	63	13.21	$3.21 \cdot 10^3$	–	5.11
LR2a	3	21	12.06	$2.99 \cdot 10^3$	6.8	5.55
LR3a	5	12.6	11.53	$2.88 \cdot 10^3$	10.3	5.76
LR4a	30	2.1	10.02	$2.56 \cdot 10^3$	20.2	6.65
LR5a	100	0.63	9.04	$2.33 \cdot 10^3$	27.4	7.36
LR6a	300	0.21	8.17	$2.13 \cdot 10^3$	33.6	7.68

The most interesting information deriving from the elaboration of response data is that the coupled spring-dampers show the same dissipation capacity of a single element, when subjected to one-half its maximum displacements and velocities, x_1 and v_1. Indeed, said c_2, x_2, and v_2 the damping coefficient, maximum displacement, and maximum velocity for the coupled devices, by equating the energies dissipated in the two series of tests:

$$4c_1 v_{1,\max}^{\alpha} x_{1,\max} = 4c_2 v_{2,\max}^{\alpha} x_{2,\max} \tag{5}$$

and substituting $x_{1,\max} = 2x_{2,\max}$ and $v_{1,\max} = 2v_{2,\max}$ in (5), the following relation between c_2 and c_1 is obtained:

$$c_2 = 2^{0.15} \cdot 2 \cdot c_1 = 2.22\, c_1 \tag{6}$$

This numerical relation is just confirmed by the ratios of the c_2 values in Table 2 to the c_1 values in Table 1, for tests LR1 and LR1a, LR2 and LR2a, LR3 and LR3a. Concerning the remaining tests, the ratios become slightly greater (from 2.46 for LR4 and LR4a, to 2.61 for LR6 and LR6a), due to some alterations caused by the strain rate effects featuring the tests with the greatest λ values. The experimental validation of relation (6) for the real-time (λ = 1) and moderately time-expanded (λ = 3, 5) tests attests the linear combination of the damping contributions of SFV dissipaters when installed in pairs.

The $F_{\max}$ values in Table 2 show similar reductions to the ones observed for a single device, as λ increases, due to the strain-rate dependent behaviour of the SFV devices. These effects can be compensated by the following force-correction expression (Molina et al., 2004):

$$F_{\lambda=1} \cong F^{c}_{\lambda=\lambda_i} = B_{\lambda_i} \cdot F_{\lambda=\lambda_i} \tag{7}$$

where $F_{\lambda=1}$ is the force measured in a real-time test, $F^{c}_{\lambda=\lambda_i}$, $F_{\lambda=\lambda_i}$ are the corrected and measured values of the force for the corresponding test carried out with $\lambda = \lambda_i$, and B_{λ_i} is the experimentally evaluated force-correction coefficient. Figure 11 shows the dependence of B_{λ_i} on λ, as determined by the results of this testing sequence.

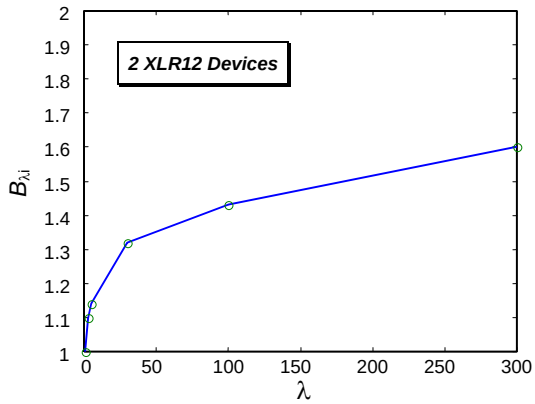

Figure 11. Force-correction coefficient as a function of λ

The effectiveness of this force-correction relation, formulated to compensate the strain rate effects in pseudodynamic tests, can be checked by comparing the response cycles obtained for λ = 1 and $\lambda = \lambda_i$, with the latter modified by (7). As way of example, this comparison is performed in Figure 12 for tests LR1a (λ = 1) and LR5a (λ = 100), by applying the coefficient value identified for λ = 100, that is, $B_{\lambda_i} = B_{100} = 1.43$.

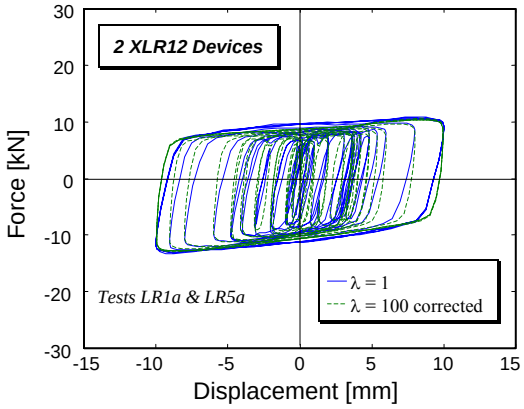

Figure 12. Response cycles obtained from tests with λ = 1, and λ = 100 after correction by (7)

3.2.2 Second series of tests

The real-time tests on the single XLR12-200 device showed a lower damping coefficient c_1 than the c value located in the design phase (2.37 against 6.1 kN(s/mm)$^{\alpha}$). This was due to the standard calibration of the piston bore of this spring-damper, as provided by the manufacturer. Then, in order to obtain the desired seismic energy dissipation in the pseudodynamic test, it was decided to modify c_1 by varying the bore of the piston heads of the two devices. By considering the friction damping contributions afforded by the sliding bearings to the response of the BISD system, which will be examined in detail in sections 3.2.3, 3.3 and 3.4, a new c_1 value of 4.7 kN(s/mm)$^{\alpha}$ was particularly requested for each spring-damper, so as to reach a global dissipation capacity of the protection system near to the global c_t design value (12.2 kN(s/mm)$^{\alpha}$).

After this modification, the two spring-dampers were subjected to a new characterisation campaign in pull-push configuration (tests LR1b → LR6b). Relevant results are recapitulated in Table 3, confirming previous observations on ΔE_d. This allowed keeping the same B_{λ_i} -λ graph plotted in Figure 11 also after the change to the piston bore.

Table 3. Test results and computed data

Test	λ	v_{max} (mm/s)	F_{max} (kN)	E_d (kN·mm)	ΔE_d (%)	c_2 (kN(s/mm)$^{\alpha}$)
LR1b	1	63	23.09	$6.06 \cdot 10^3$	–	9.46
LR2b	3	21	20.71	$5.72 \cdot 10^3$	5.6	10.67
LR3b	5	12.6	19.93	$5.54 \cdot 10^3$	8.6	10.98
LR4b	30	2.1	17.62	$4.94 \cdot 10^3$	18.5	12.95
LR5b	100	0.63	16.14	$4.46 \cdot 10^3$	26.4	13.96

The real-time tests attested the achievement of the new target value of the damping coefficient. Indeed, c_2 was just twice the requested value for each device. Similarly to Figure 12 for tests LR1a and LR5a, the response cycles obtained from tests LR1b and LR5b – with the latter amplified by $B_{\lambda_i} = B_{100} = 1.43$ – are drawn in Figure 13. A

satisfactory compensation of strain-rate effects is clearly ensured by (7) also for this new testing sequence.

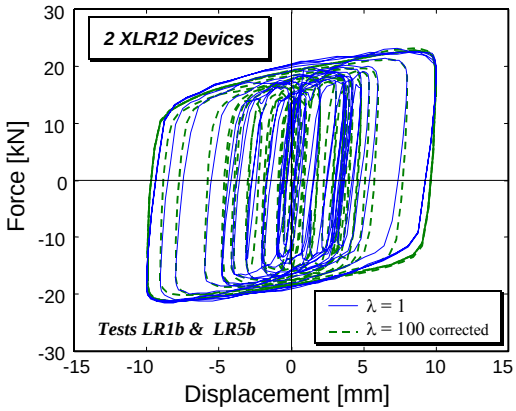

Figure 13. Response cycles obtained from tests with λ = 1, and λ = 100 after correction by (7)

3.3 Tests on steel-Teflon sliding bearings

The steel-Teflon sliders were tested by the apparatus in Figure 7, prior to connect the spring-dampers. A scheme of this reduced set-up is shown in Figure 14.

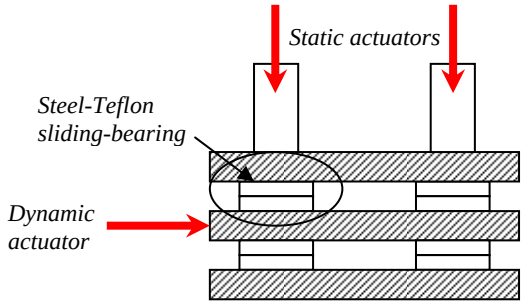

Figure 14. Scheme of the experimental set-up for tests on the sliding bearings alone

The equivalence of the compression stress state on the four Teflon disks incorporated in this set-up, and the three disks designed to be ideally placed at the base of the three columns of each frame constituting the steel mock-up, was ensured by assuming a ¾ area for the disks of the tested sliders.

The cyclic tests were carried out at the same six velocities imposed to the Jarret devices. In the case of the sliders, a further input variable was represented by the vertical load applied by the static actuators. Four total vertical loads were particularly assumed: N_{tot} = 32, 78, 196, and 275 kN. This gave rise to the following load shares N_i on each of the four bearings, aligned in pairs along the vertical axis: N_i = 16, 39, 98, and 137.5 kN. Given $F_{h,mean}$ the mean value of the horizontal force measured on the plateau branches of the response cycles, the friction coefficient μ was computed as:

$$\mu = \frac{F_{\mathrm{h,mean}}}{4N_{\mathrm{i}}} \tag{8}$$

In addition to μ, the equivalent viscous damping coefficient c_{eq} that should have a SFV device – characterised by a fractional exponent $\alpha = 0.15$ – to produce the same energy dissipation of a steel-Teflon slider, was also calculated. The experimental data, as well as the μ and c_{eq} values derived from this computation, are summed up in Table 4 for the twenty-four tests performed.

Table 4. Test results and computed data

Test	λ_i	v_{max} (mm/s)	$F_{h,mean}$ (kN)	E_d (kN·mm)	N_i (kN)	μ (%)	c_{eq} (kN(s/mm)$^{\alpha}$)
d141	1	63	1.60	$0.66 \cdot 10^3$	16	2.50	1.04
d142	3	21	1.60	$0.65 \cdot 10^3$	16	2.50	1.20
d143	5	12.6	1.61	$0.66 \cdot 10^3$	16	2.51	1.33
d144	30	2.1	1.63	$0.68 \cdot 10^3$	16	2.54	1.79
d145	100	0.63	1.61	$0.67 \cdot 10^3$	16	2.51	2.10
d146	300	0.21	1.59	$0.64 \cdot 10^3$	16	2.48	2.41
d147	1	63	3.26	$1.36 \cdot 10^3$	39	2.09	2.10
d148	3	21	3.26	$1.37 \cdot 10^3$	39	2.09	2.49
d149	5	12.6	3.26	$1.35 \cdot 10^3$	39	2.09	2.71
d150	30	2.1	3.30	$1.39 \cdot 10^3$	39	2.11	3.66
d151	100	0.63	3.27	$1.38 \cdot 10^3$	39	2.09	4.35
d152	300	0.21	3.20	$1.32 \cdot 10^3$	39	2.05	4.98
d153	1	63	6.28	$2.71 \cdot 10^3$	98	1.60	4.24
d154	3	21	6.22	$2.66 \cdot 10^3$	98	1.58	4.93
d155	5	12.6	6.17	$2.65 \cdot 10^3$	98	1.57	5.28
d156	30	2.1	6.17	$2.65 \cdot 10^3$	98	1.57	6.94
d157	100	0.63	6.13	$2.64 \cdot 10^3$	98	1.56	8.27
d158	300	0.21	6.05	$2.63 \cdot 10^3$	98	1.54	9.73
d159	1	63	8.18	$3.77 \cdot 10^3$	137.5	1.48	5.91
d160	3	21	8.03	$3.65 \cdot 10^3$	137.5	1.46	6.76
d161	5	12.6	8.06	$3.57 \cdot 10^3$	137.5	1.46	7.10
d162	30	2.1	8.16	$3.59 \cdot 10^3$	137.5	1.48	9.39
d163	100	0.63	8.20	$3.65 \cdot 10^3$	137.5	1.49	11.44
d164	300	0.21	8.01	$3.70 \cdot 10^3$	137.5	1.45	12.98

The results in Table 4 show that $F_{h,mean}$, and thus μ, are practically independent from velocity, except for a very slight reduction for quasi-static response conditions ($\lambda = 300$), as observed in Sorace and Terenzi (2004). At the same time, μ is confirmed to be an inverse function of the normal stress f_n. On the whole, the low μ values obtained in relation to the low-to-moderate f_n values applied (ranging from 1.1 MPa – N_i =16 kN, to 9.2 MPa – N_i = 137.5 kN) underline a good performance of the sliders, which largely met the requirements of CNR-10018-98 (1999) and prEN-1337 (2003), as well as of the new Italian Seismic Standards (OPCM/3431, 2005). The response cycles obtained from the

four tests with $\lambda = 1$, and the corresponding μ coefficient time-histories are demonstratively plotted in Figures 15 and 16.

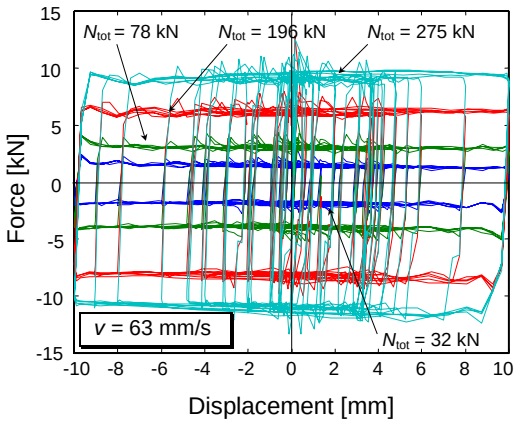

Figure 15. Response cycles obtained from tests at the maximum velocity, for the four vertical loads applied

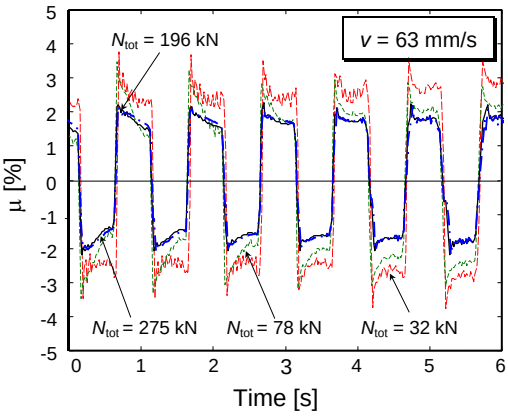

Figure 16. Friction coefficient time-histories obtained from tests at the maximum velocity, for the four vertical loads applied

3.4 Tests on the BISD system

Several series of tests were carried out on the BISD system, with the Jarret spring-dampers in their first and second piston-bore configuration. The results of the testing sequence performed with the SFV devices characterised by the c_2 damping coefficients in Table 3, are presented in this section. The vertical load coincided with the maximum value imposed to the sliders (N_{tot} = 275 kN, N_i = 137.5). In this case, the tests were limited to the first five velocities previously adopted ($\lambda = 1 \rightarrow 100$). Results are listed in Table 5, along with the values of the equivalent damping coefficient $c_{eq,tot}$ calculated, according to model (3), for the complete BISD system. The $c_{eq,tot}$ data in Table 5 were then compared with the sum of the damping contributions derived from the corresponding tests on the spring-dampers (LR1b $\rightarrow$ LR5b), and the sliders – with N_{tot} = 275 kN (d159 $\rightarrow$ d163) –, separately carried out. The c_{eq} values evaluated in the tests on the sliders with N_i = 16 kN (d141 $\rightarrow$ d145) were deducted from this sum, to eliminate this friction damping contribution from the response of the dissipaters in tests LR1b through LR5b.

Table 5. Test results and computed data

Test	λ	v_{max} (mm/s)	F_{max} (kN)	E_d (kN·mm)	N_i (kN)	$c_{eq,tot}$ (kN(s/mm)$^\alpha$)
d185	1	63	31.51	$9.01 \cdot 10^3$	137.5	14.03
d186	3	21	28.78	$8.62 \cdot 10^3$	137.5	16.09
d187	5	12.6	28.13	$8.40 \cdot 10^3$	137.5	16.72
d188	30	2.1	26.09	$7.88 \cdot 10^3$	137.5	20.48
d189	100	0.63	24.22	$7.51 \cdot 10^3$	137.5	23.43

The following coefficients were obtained:

$c_{eq,sum}$(LR1b, d159, d141) = c_1(LR1b) + c_{eq}(d159) - c_{eq}(d141) = 14.30 kN(s/mm)$^\alpha$

$c_{eq,sum}$(LR2b, d160, d142) = c_1(LR2b) + c_{eq}(d160) - c_{eq}(d142) = 16.23 kN(s/mm)$^\alpha$

$c_{eq,sum}$(LR3b, d161, d143) = c_1(LR3b) + c_{eq}(d161) - c_{eq}(d143) = 16.75 kN(s/mm)$^\alpha$

$c_{eq,sum}$(LR4b, d162, d144) = c_1(LR4b) + c_{eq}(d162) - c_{eq}(d144) = 20.55 kN(s/mm)$^\alpha$

$c_{eq,sum}$(LR5b, d163, d145) = c_1(LR5b) + c_{eq}(d163) - c_{eq}(d145) = 23.3 kN(s/mm)$^\alpha$

which practically coincide with the $c_{eq,tot}$ values for the corresponding velocities.

Similar evaluations were developed also in terms of damping energy E_d:

E_d(LR1b, d159, d141) = E_d(LR1b) + E_d(d159) - E_d(d141) = $9.17 \cdot 10^3$ kN·mm

E_d(LR2b, d160, d142) = E_d(LR2b) + E_d(d160) - E_d(d142) = $8.72 \cdot 10^3$ kN·mm

E_d(LR3b, d161, d143) = E_d(LR3b) + E_d(d161) - E_d(d143) = $8.45 \cdot 10^3$ kN·mm

E_d(LR4b, d162, d144) = E_d(LR4b) + E_d(d162) - E_d(d144) = $7.85 \cdot 10^3$ kN·mm

E_d(LR5b, d163, d145) = E_d(LR5b) + E_d(d163) - E_d(d145) = $7.44 \cdot 10^3$ kN·mm

showing the same level of correlation with the E_d values in Table 5.

These data asserts that, within the limits imposed by the experimental accuracy, the sum of the contributions of the spring-dampers and the sliders taken separately coincides with the corresponding global measure for the assembled BISD system, both in terms of damping coefficients and dissipated energies.

As for the other experimental sections, the tests were reproduced numerically. The $c_{eq,tot}$ coefficient defined for the BISD system was introduced in equation (3) within these analyses, developed by the equivalent model of the spring-dampers inclusive of the friction damping contributions of the sliders, as an alternative to an in-parallel combination of the numerical models of the two types of devices. Comparison with test results is demonstratively offered in Figure 17, in terms of reaction force time-histories, force-displacement cycles, and damping energy time-histories, for the λ = 1 test (d185). The satisfactory correlation of numerical and experimental responses allowed assessing the simulation capacities of the adopted model also in the application to the complete BISD system.

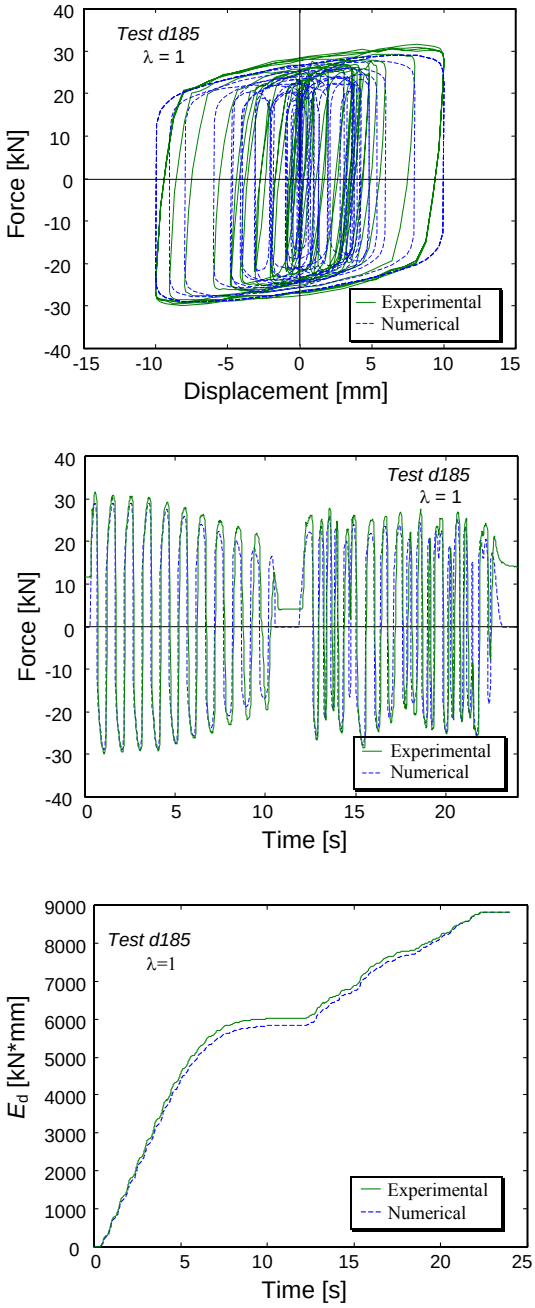

Figure 17. Experimental reaction force time-history, force-displacement cycles and damping energy time-history, and relevant numerical simulations, for d185 test

4 SUBSTRUCTURED PSEUDODYNAMIC TEST

4.1 Description of the testing method

The applied pseudodynamic testing procedure is based on a step-by-step integration of the equation of motion formulated for the global system, composed by the superstructure and the isolation level:

$$\mathbf{Ma}+\mathbf{r}=\mathbf{p} \tag{9}$$

There, the theoretical mass matrix $\mathbf{M}$ includes the mass of the base as well as the masses of the storeys, and $\mathbf{a}$ is the acceleration vector that contains the relative accelerations at the base and all the storeys. Then, $\mathbf{p}$ is the specified external force vector, constituted by the equivalent seismic loads that are proportional to the ground accelerogram.

The substructuring is introduced in the pseudodynamic procedure by the decomposition of the restoring force vector into two terms:

$$\mathbf{r}=\mathbf{r}_{\mathrm{se}}+\mathbf{r}_{\mathrm{is}} \tag{10}$$

The first term in this equation contains the restoring forces coming from the elements of the superstructure, and is linearly modelled by the theoretical damping $\mathbf{C}_{\mathrm{se}}$ and stiffness $\mathbf{K}_{\mathrm{se}}$ matrices of the superstructure as

$$\mathbf{r}_{\mathrm{se}}=\mathbf{C}_{\mathrm{se}}\mathbf{v}+\mathbf{K}_{\mathrm{se}}\mathbf{d} \tag{11}$$

There, $\mathbf{v}$ and $\mathbf{d}$ are the relative velocities and displacements at all the storeys, respectively. Then, the second term in (11) contains the restoring force at the isolation system in the experimental set-up r_{is}, which is assembled at the base degree of freedom, and zeroes at the superstructure positions

$$\mathbf{r}_{\mathrm{is}}=\begin{bmatrix} r_{\mathrm{is}} \\ \mathbf{0} \end{bmatrix} \tag{12}$$

Since the pseudodynamic test is performed at a speed much lower than the real one, a strain-rate-effect compensation on the measured force may be appropriate as the one mentioned in section 3.2.1 for the adopted spring-dampers (Molina et al., 2004), i.e.,

$$r_{\mathrm{is}}=B_{\lambda_{\mathrm{i}}}\cdot r_{\mathrm{is}}^{\mathrm{meas}} \tag{13}$$

where $r_{\mathrm{is}}^{\mathrm{meas}}$ is the measured force at the load cell of the actuator, and the force-correction coefficient $B_{\lambda_{\mathrm{i}}}$ is fixed by the graph in Figure 11 according to the selected testing speed λ_{i}. Depending on the complexity of the model for the restoring forces of the superstructure, several testing algorithms and computing hardware configurations are available at ELSA that, for example, may even allow for non-linear finite-element models with a high number of degrees of freedom, and working in networked computers at different laboratories ("distributed" substructure technique). In those complex cases, the integration algorithm allows for the use of a larger time increment at the numerical substructure, while for the experimental substructure a smaller one is kept to reduce the experimental errors coming from any discontinuity in the movement.

As an alternative to the mentioned distributed technique, the testing method applied to the current problem was the "monolithic" substructure technique in which all the substructures, experimental or numerical, are managed at an only master CPU that arranges all the parameters in the equation of motion (9), and integrates it with a time

increment common to all the substructures. Moreover, the continuous pseudodynamic technique was applied, which is based on the use of hundreds of time steps at every second of the laboratory time. By updating the computed reference with such a high sampling frequency, the control system has no possibility to induce oscillation within every step, which avoids the need for a stabilising lapse before taking the measure. This time step is typically of 2ms, which is coincident with the sampling frequency of the controller. By way of example, if the testing speed is $\lambda_i = 100$, the integration time increment in the accelerogram would be 2ms/100=20μs, for which the numerical stability and accuracy of the integration is guaranteed for the Explicit Newmark Method. Since by adopting a similar time step, the response is obtained at even millions of time instants, it is preferable to reduce those to a few thousands instants representing the averages of the original ones. This operation also reduces the noise of the original measures. Finally, as a consequence of the elimination of the stabilising and averaging lapses within every step, the use of the continuous PsD technique generally allows for testing speeds which can be faster, by one order of magnitude, than the ones performed by the classical step-by-step technique. Apart from some other practical advantages, the increase in testing speed may also help to reduce the induced strain-rate effects.

4.2 Results and elaborations

As premised in section 2, the pseudodynamic test was carried out by using the accelerogram in Figure 2 as input. The experimental response is illustrated in Figures 18 through 20, where the base displacement time-history (Figure 18), base shear-base displacement cycles (Figure 19), and story-displacement time-histories (Figure 20) are plotted in superimposition to relevant numerical simulations. The values of the model parameters used in this analysis were drawn from a best fitting process on the experimental results.

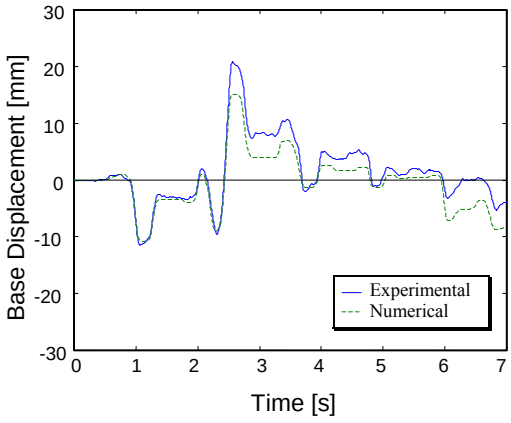

Figure 18. Pseudodynamic test: base displacement time-histories, and relevant numerical simulation

A $c_{eq,tot}$ coefficient equal to 13 kN(s/mm)$^{\alpha}$, and a k_2 stiffness of 0.35 kN/mm were particularly identified by this process. The latter is very close to the stiffness value established for the coupled spring-dampers in the preliminary design phase (k_{2t} = 0.356 kN/mm, section 2), to obtain the target fundamental frequency f_{is} = 0.704 Hz. The experimentally measured frequency was equal to 0.685 Hz, exactly corresponding to the

identified k_2 value. Concerning the post-calculated $c_{eq,tot}$ coefficient, this is consistent with the results of tests reported in sections 3.2.2 and 3.3, as illustrated in the following.

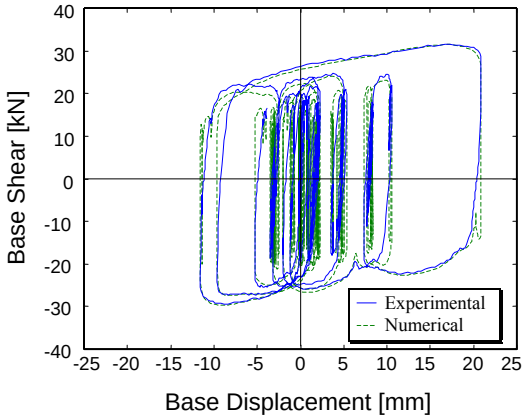

Figure 19. Pseudodynamic test: base shear-base displacement cycles, and relevant numerical simulation

The weight of half structure considered in the pseudodynamic test is equal to 178.8 kN, 50% of which transferred to the central bearing (89.4 kN) and 25% to each lateral bearing (44.7 kN). These loads are not very different from the N_{tot} values applied in the real-time tests d147 (78 kN) and d141 (32 kN), respectively, on the sliders (section 3.3). By summing relevant c_{eq} coefficients in Table 4 to the c_2 value in Table 3 for λ =1, $c_{eq,tot}$ = 13.6 kN(s/mm)$^{\alpha}$ is obtained, very similar to the coefficient identified from the pseudodynamic test. These findings are further confirmed by the results of the real-time test d153, carried out with N_{tot} = 196 kN, for which c_{eq} = 4.24 kN(s/mm)$^{\alpha}$ is found, giving rise to a $c_{eq,tot}$ = 13.74 kN(s/mm)$^{\alpha}$ total equivalent damping coefficient.

Figure 21 shows the energy time-histories obtained from the pseudodynamic test, being E_i the input energy, $E_{d,v}$ the viscous damping energy dissipated by the SFV devices, and $E_{d,f}$ the friction damping energy dissipated by the sliding bearings. The energy response highlights a 84% share of dissipation for the SFV devices, and a 16% share for the sliders. This provides an indication about the two percentile contributions, which are anyway strictly related to the specific characteristics of any single case study. As a different way of example, the energy shares evaluated for the actual reinforced concrete building analysed in (Sorace and Terenzi, 2004, 2005) are approximately equal to 90% for the spring-dampers, and 10% for the sliders.

The benefits provided by the BISD system are visually represented in Figure 22, where the interstory drift time-histories are compared with the ones obtained from the pseudodynamic test carried out in unprotected conditions, for the same input accelerogram, within DISPASS (Sorace and Terenzi, 2003, Molina et al., 2004). The maximum drift values $I_{d1,max}$, $I_{d2,max}$ and $I_{d3,max}$ are listed in Table 6 for the two configurations, showing 3.63, 3.42, and 3.23 reduction factors, for the first, second, and third story, in passing from fixed-base to base-isolated conditions.

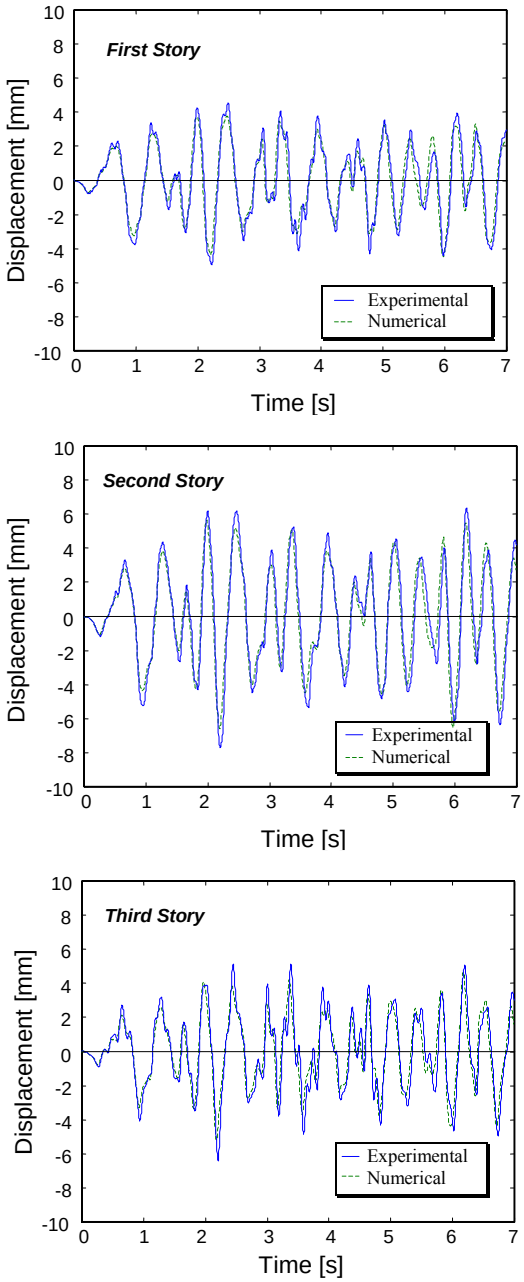

Figure 20. Pseudodynamic test: story displacement time-histories, and relevant numerical simulations

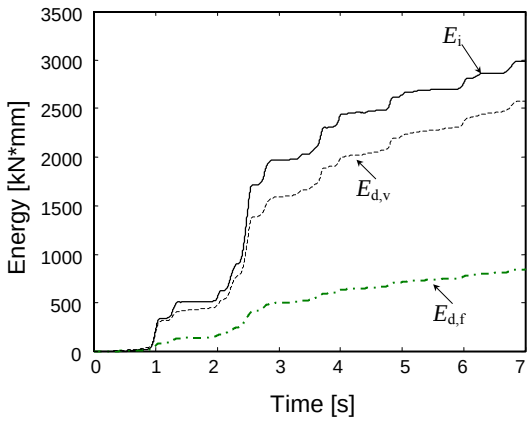

Figure 21. Pseudodynamic test: energy time-histories

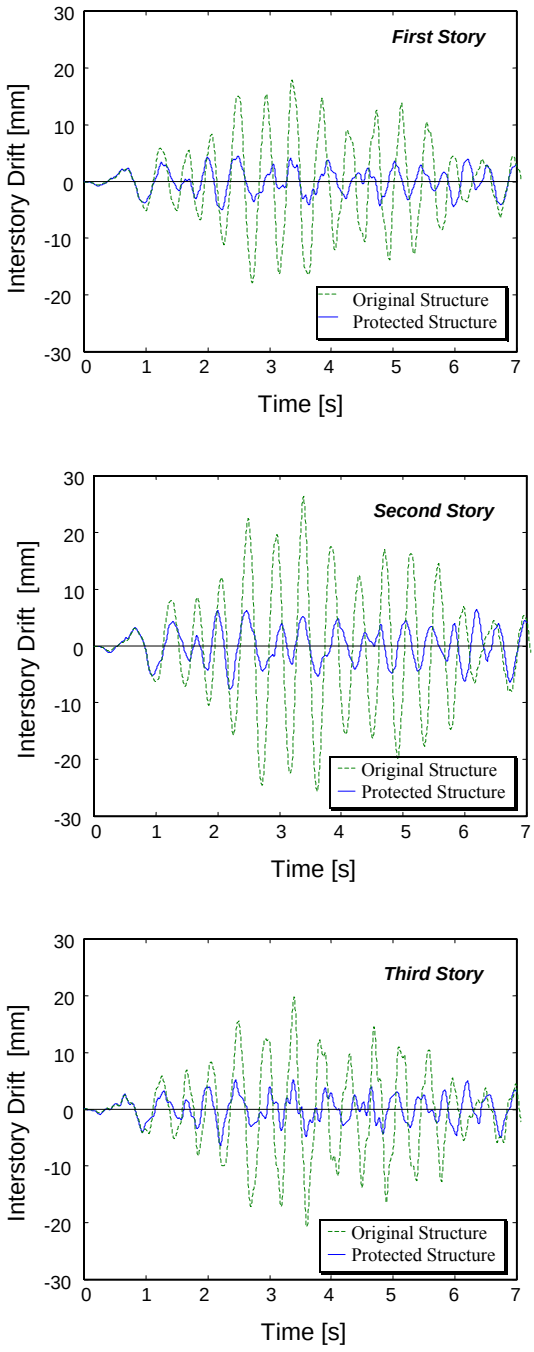

Figure 22. Interstory drift time-histories obtained from the pseudodynamic tests on the steel structure in original and protected conditions

Table 6. Maximum interstory drifts obtained from the pseudodynamic tests on the steel structure in original and protected conditions

Mock-up Configuration	$I_{d1,max}$ (mm)	$I_{d2,max}$ (mm)	$I_{d3,max}$ (mm)
Original	17.8	26.3	20.7
Protected	4.9	7.7	6.4

This remarkable improvement leads to interstory drift ratios of 2.5‰, 3.4‰, and 3.2‰ for the first, second, and third story, respectively, which are neatly below the 5‰ limit corresponding to the highest performance level postulated for retrofitted steel frames ("operational level"), under the basic design earthquake, in international performance-based design documents, among which FEMA-356 (2003). This is the consequence of the beneficial action of base isolation, as well as of the additional damping supplied by the adopted dissipaters. The latter also ensures an optimal control of base displacements, constrained within 20.9 mm, as illustrated in Figures 18 and 19.

5 CONCLUSIONS

The experimental research presented in this report allowed reaching the objectives formulated for the DISPASS Project section dedicated to the analysis of the BISD system, as summed up below.

– Elaboration of test results in terms of energy balance and damping coefficients allowed verifying the additive combination of the dissipative action of the SFV devices when mounted in pairs, as well as of their viscous damping with the frictional damping of steel-Teflon sliding bearings, within a BISD installation.

– A "global" equivalent damping coefficient was formulated for the system, starting from its definition for the SFV spring-dampers. Moreover, a new calibration of the force correction expression for the strain rate effects, as included in the ELSA pseudodynamic testing procedure, was developed for the devices experimented in this project.

– Further experimental validation of the analytical and numerical models adopted for the SFV Jarret dissipaters was obtained.

– The enhancement of seismic response provided by the considered protection technology was assessed by comparison with the results of the pseudodynamic test previously carried out, with the same input earthquake, on the reference steel structure in fixed-base configuration. Reduction factors greater than 3 were particularly observed in terms of interstory drifts, in passing from original to protected conditions.

– In addition to the noticeable enhancement of superstructure response, the highly nonlinear viscous damping action of the SFV devices allowed constraining also the base displacements within very low limits, as implicitly imposed by the design equation by which the *c* coefficient of the spring-dampers was preliminarily evaluated.

5 REFERENCES

Chiarugi, A., Sorace, S., Terenzi, G. (2000). Application of a design method for FV dampers in base-isolation systems, *Proc., Final Workshop on the Italian National Research Project "Protezione sismica dell'edilizia esistente e di nuova edificazione attraverso sistemi innovativi"*, Naples, Italy, May 12-13, 2000, A. De Luca Ed., 82-95.

Chiarugi, A., Sorace, S., Terenzi, G. (2001). Metodo di progetto di dispositivi siliconici per l'isolamento alla base: applicazione a due casi sperimentali [Design method for silicone-fluid devices in base isolation: Application to two experimental case-studies], *Proc., 10th Italian National Conference on Earthquake Engineering*, Potenza-Matera, September 9th-13th, 2001, CD-ROM (in Italian).

FEMA 356 (2000). Prestandard and commentary for the seismic rehabilitation of buildings, *Building Seismic Safety Council*, FEMA, Washington, DC.

Molina, F.J., Sorace, S., Terenzi, G. Magonette, G., Viaccoz, B. (2004). Seismic tests on reinforced concrete and steel frames retrofitted with dissipative braces. *Earthquake Engineering and Structural Dynamics*, Wiley&Sons Ltd, 33, 1373-1394.

OPCM/3431 (2005). Norme tecniche per il progetto, la valutazione e l'adeguamento sismico degli edifici [Technical Standards for the design, evaluation and seismic retrofit of buildings], G.U. May 3rd, 2005, Rome, Italy.

CNR 10018 (1999). Apparecchi di appoggio per le costruzioni. Istruzioni per l'impiego [Bearing devices for structures. Instructions for use], CNR, Bollettino Ufficiale, Rome, Italy.

prEN 1337 (2003). Structural bearings, CEN – European Committee for Standardization, Final draft.

Schmidt, K., Dorka, U.E., Taucer, F., Magonette, G. (2004). Seismic retrofit of a steel frame and a R/C frame with HYDE systems, *Publication EUR 21180 EN, European Commission – Joint Research Centre*, Institute for the Protection and Security of the Citizen/European Laboratory for Structural Assessment, Ispra, Italy.

Sorace, S., Terenzi, G. (2001a). Non-linear dynamic modelling and design procedure of FV spring dampers for base isolation, *Engineering Structures*, Elsevier Science Ltd, 23, 1556-1567.

Sorace, S., Terenzi, G. (2001b). Non-linear dynamic design procedure of FV spring-dampers for base isolation – Frame building applications, *Engineering Structures*, Elsevier Science Ltd, 23, 1568-1576.

Sorace, S., Terenzi, G. (2003). Large-scale experimental validation of a design procedure for damped braced steel structures, *Proc., STESSA 2003 – 4th International Conference on the Behaviour of Steel Structures in Seismic Areas*, Naples, Italy, A A Balkema, Lisse, 657-662.

Sorace, S., Terenzi, G. (2004). Analisi progettuale di un edificio dotato di dispositivi fluido-viscosi ed appoggi scorrevoli alla base [Design analysis of a building incorporating fluid-viscous devices and sliding bearings at its base], *Proc., 15th CTE Congress*, Bari, November 4th-6th, 2004, 651-660 [in Italian].

Sorace, S., Terenzi, G. (2005). Application of a combined base isolation/supplemental damping seismic protection strategy to a public building in Florence, *Proc., International Conference "250th Anniversary of the 1755 Lisbon Earthquake"*, Lisbon, November 1-4, 2005, 481-486.

Terenzi, G (1999). Dynamics of SDOF systems with nonlinear viscous damping, *Journal of Engineering Mechanics*, ASCE, 125, 956-963.

European Commission

EUR 22147 EN – DG Joint Research Centre, Institute for the Protection and Security of the Citizen

Luxembourg: Office for Official Publications of the European Communities
2006 – 23 pp. – 21 x 29.7 cm
Scientific and Technical Research series

Abstract

An experimental investigation was carried out on an advanced seismic protection system incorporating base isolators and supplemental damping devices. This testing campaign was part of the Research Programme DISPASS (Dissipation and ISolation PAssive Systems Study), financed under the ECOLEADER contract within the Fifth Framework Program of the European Commission. The protection strategy considered herein consists in coupling stainless steel-Teflon bearings, operating as sliders, and silicone fluid viscous spring-dampers. The latter are connected to the base-floor of the isolated building to provide the desired passive control of superstructure response, as well as to guarantee its complete re-centring after termination of a seismic action. Two types of experiments were conducted: sinusoidal and random cyclic tests, and a pseudodynamic test in “substructured” configuration. The cyclic tests were aimed at characterising the hysteretic response of the spring-dampers, the frictional behaviour of the steel-Teflon bearings, and the combined response of their assembly. The pseudodynamic test simulated the installation of the protection system at the base of a three-story steel frame structure, physically tested in other tasks of the DISPASS Project in unprotected conditions, as well as by equipping it with different passive control technologies. The results of the performed tests, as well as of relevant mechanical interpretation and numerical simulation analyses, are presented in this report.

EUROPEAN COMMISSION
DIRECTORATE-GENERAL
Joint Research Centre

The mission of the Joint Research Centre is to provide customer-driven scientific and technical support for the conception, development, implementation and monitoring of European Union policies. As a service of the European Commission, the JRC functions as a reference centre of science and technology for the Union. Close to the policy-making process, it serves the common interest of the Member States, while being independent of special interests, whether private or national.